

# Direct measurement of the camel-back energy surface in AIAs and its evolution in an electric field

Hyunsik Im,\* L. E. Bremme, and P. C. Klipstein†

*Clarendon Laboratory, Department of Physics, University of Oxford, Parks Road, Oxford, OX1 3PU, United Kingdom*

A. V. Kornilov

*Lebedev Physical Institute, Moscow, 117924, Russia*

H. Beere and D. Ritchie

*Semiconductor Physics Group, Cavendish Laboratory, Madingley Road, Cambridge CB3 0HE, United Kingdom*

R. Grey and G. Hill

*EPSRC III-V Facility, Department of Electrical and Electronic Engineering, University of Sheffield, Mappin Street, Sheffield S1 3JD, United Kingdom*

(Received 9 October 2003; published 10 November 2004)

We report the direct measurement of the AIAs conduction band dispersion near the band edge. The six lobes of its constant energy surface are much more spherical than previously supposed, with a ratio of major to minor axes of less than 2. The existence of a “camel back” is confirmed. The  $\mathbf{k}\cdot\mathbf{p}$  interaction responsible for the camel back is found to be about three times the presently accepted value. A consequence is that above some critical electric field applied perpendicular to an AIAs quantum well, the sub-band constant energy surface is rotated by  $45^\circ$ . We confirm this behavior experimentally in the same sample.

DOI: 10.1103/PhysRevB.70.205313

PACS number(s): 73.21.Fg, 73.40.Gk, 71.18.+y

## I. INTRODUCTION

Due to the importance of silicon as the key semiconductor in modern integrated circuits, and more recently, of  $\text{Ga}_{1-x}\text{Al}_x\text{As}$  as one of the key materials in opto-electronics, the similar character of their electron constant energy surfaces (for  $x > 0.4$ ) has become almost a trademark of traditional semiconductor physics, appearing in many textbooks. This constant energy surface is characterized by six ellipsoids pointing in the positive and negative  $\langle 100 \rangle$  directions, near the  $X$ -point faces of the Brillouin zone, which we label (in pairs):  $X_X$ ,  $X_Y$ , and  $X_Z$ .

The ellipsoidal shape of this characteristic constant energy surface was predicted theoretically many years ago.<sup>1,2</sup> It can be influenced by a “camel-back” dispersion that may strongly enhance the anisotropy of each ellipsoid. The camel back is caused by the  $\mathbf{k}\cdot\mathbf{p}$  interaction between bands of  $X_1$  and  $X_3$  symmetry that lie close in energy (see the inset to Fig. 1). In AIAs, these bands are separated by 0.35 eV. However, even though  $X$  electrons in AIAs can sometimes affect the performance of modern devices such as quantum cascade lasers,<sup>3</sup> it is still not clear whether or not the camel back actually exists in this material. On the other hand, the ellipsoids in silicon are known to be very anisotropic, and the existence of a camel back is more certain.<sup>4</sup> Notably, the anisotropy has recently received much attention after its exploitation in strained field effect transistors led to a new record in transistor operating speed.<sup>5</sup>

In  $\text{Ga}_{1-x}\text{Al}_x\text{As}$ , for  $x > 0.4$ , there has been much theoretical work to try and establish the exact shape of the ellipsoids. Major to minor axis ratios of between 2.4 and 7 have been predicted for AIAs.<sup>6-8</sup> On the other hand, until now it has

been very hard to measure the shape experimentally. There exists only one report, based on complex modeling of time-resolved photoluminescence measurements from electron-hole droplets,<sup>2</sup> which predicted a large ratio of  $\sim 4.5$ . In the present work we shall demonstrate that the above picture of strongly anisotropic ellipsoids is incorrect. We present direct measurement of the axis ratio, using magneto-tunneling between  $X_{X,Y}$  states in AIAs quantum wells grown in the  $z$  direction. We show that for a constant energy surface with wave vectors in the range of  $0.02 \times 2\pi/a_0$  ( $a_0$  is the cubic lattice parameter) the ratio is in fact much closer to unity

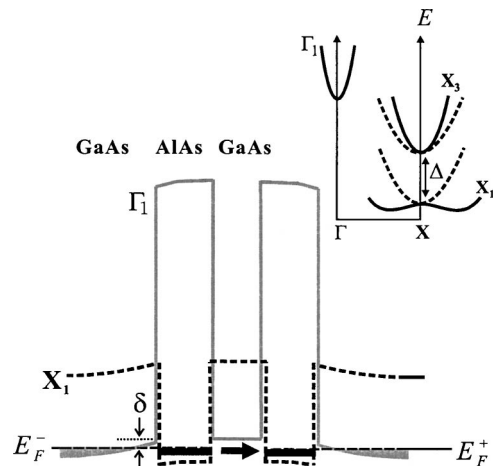


FIG. 1. The  $\Gamma_1$  and  $X_1$  conduction band profiles at  $P > 10$  kbar and zero bias. Inset: Schematic diagram showing  $\mathbf{k}\cdot\mathbf{p}$  induced repulsion between  $X_1$  and  $X_3$  states leading to the camel-back dispersion.

than previously supposed. The AIAs constant energy surface ellipsoids are thus almost spherical, quite unlike the case of silicon. Such a small ratio causes us to completely re-evaluate the presently accepted  $\mathbf{k}\cdot\mathbf{p}$  parameters for AIAs. Our values provide strong confirmation of the existence of a camel back, even in the absence of strongly anisotropic ellipsoids, but change its depth and position substantially.

We find that the size of the  $\mathbf{k}\cdot\mathbf{p}$  interaction parameter is strongly increased, approximately by a factor of 3 compared to the previously accepted value. This increase greatly enhances the influence of a band-mixing effect<sup>9,10</sup> between the  $X_X$  and  $X_Y$  ground states in AIAs quantum wells to the point where the effect can be observed experimentally, as a dramatic realignment of the constant energy surface when a strong electric field is applied perpendicular to the well. We have measured the constant energy surface directly as a function of increasing electric field, and now demonstrate the realignment unambiguously in the same sample.

This paper is organized as follows. In Sec. II A we present dispersion anisotropy measurements in GaAs/AIAs structures at high pressure, using resonant magneto-tunneling with the magnetic field parallel to the layer. We compare these results with our earlier high-pressure resonant magneto-tunneling measurements with the magnetic field perpendicular to the layer and with cyclotron resonance measurements in AIAs by other workers. We fit all three sets of results to just one set of  $\mathbf{k}\cdot\mathbf{p}$  parameters, which we therefore propose as new values. Section II A closes with a discussion of the implications of the new parameter values on the camel back and a proof of its existence. In Sec. II B we demonstrate the relationship between the new  $\mathbf{k}\cdot\mathbf{p}$  parameter values and the observation of interface induced  $X_X$ - $X_Y$  mixing. Finally, we draw conclusions in Sec. III.

## II. RESULTS AND ANALYSIS

### A. Determination of the camel back

GaAs/AIAs “double barrier” structures were grown with 60 or 70 Å wide AIAs *wells* separated by a 40 Å wide GaAs *barrier*. The growth details have already been reported in Ref. 11, together with resonant tunneling results that clearly demonstrate the quantum confinement in the AIAs layers and testify to the high quality of the structures. Pressure was generated by a miniature (22 mm diameter) cell that could be rotated inside a 15 T superconducting magnet. All other experimental details are similar to those of Ref. 12.

Figure 1 shows the  $X_1$  and  $\Gamma$  profiles in a double barrier structure at zero bias and above the type II transition pressure of approximately  $\sim 10$  kbar (the precise value depends on the AIAs layer widths<sup>11</sup>). At this pressure the  $X_{X,Y}$  ground states in the AIAs wells are populated by transfer of  $\Gamma$  electrons from the neighboring GaAs layers. In the figure, resonant  $2D \rightarrow 2D$  tunneling is shown between emitter and collector  $X_{X,Y}(1)$  states. Direct and phonon assisted resonances,  $X_{X,Y}(1) \rightarrow X_{X,Y}(m)$ , can also be observed with  $m=1, 2$ , or  $3$ , and have previously been described in detail in Ref. 11.

The application of an in-plane magnetic field to coupled double-quantum-well structures modifies the tunneling due to the action of the Lorentz force. If the separation between

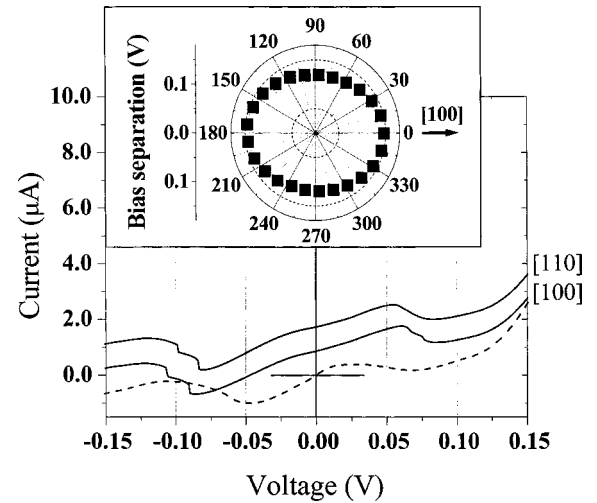


FIG. 2. The  $X_{XY}(1) \rightarrow X_{XY}(1)$  resonance in a 70–40–70 sample at 4.2 K and 9 kbar, measured at zero magnetic field (dash) and at an in-plane magnetic field of 15 T (solid) parallel to [100] and [110]. Inset: The bias separation between forward and reverse bias peaks plotted as a function of the field angle.

wells is less than the cyclotron radius, a wave-vector shift,  $\Delta k$ , is generated between initial and final resonant states. Since the initial states often occupy only a small region of  $k$  space due to a low degree of band filling, the resonance voltage is increased approximately by the dispersion energy at wave vector  $\Delta k$  of the band containing the final states. For example, if the in-plane magnetic field is oriented in the  $x$  direction, the change in wave vector for electrons tunneling over a distance  $\Delta z$  is in the  $y$  direction and is given by  $-\Delta k_y = (e/\hbar)B_x \cdot \Delta z$ . More generally, if  $\Delta \mathbf{z}$  is the separation between ground state wave functions in the emitter and collector quantum wells, the field causes a shift,  $\Delta \mathbf{k} = (e/\hbar)\mathbf{B} \times \Delta \mathbf{z}$ .<sup>13,14</sup>

Figure 2 shows the  $m=1$  resonance of a 70–40–70 sample at 4.2 K and 9 kbar, in zero magnetic field (dashed) and for in-plane fields of 15 T aligned along [100] and [110], respectively. In zero field a weak resonance,  $X_{X,Y}(1) \rightarrow X_{X,Y}(1)$ , is observed at small bias values in each direction, although the in-plane wave vector is not conserved (except at zero bias).<sup>15</sup> In a magnetic field, however, the wave vector can be conserved due to the wave-vector shift caused by the Lorentz force, whose magnitude at 15 T is  $\Delta k = 0.020 \times$  and  $0.022 \times 2\pi/a_0$  for 60–40–60 and 70–40–70 samples, respectively. The magnetic field shifts the  $m=1$  resonance bias away from zero because a finite bias is now required to achieve resonant alignment between occupied emitter and empty collector states. For a perfectly symmetric structure, the bias dropped between emitter and collector AIAs layers is proportional to the reciprocal in-plane effective mass of the collector state in a direction perpendicular to the field. The small difference between forward and reverse bias values seen in Fig. 2 has been discussed previously<sup>11</sup> and is caused by small differences in the thickness of the two AIAs layers. This effect can be eliminated by taking the average of the absolute forward and reverse bias values, as we have done in the inset of Fig. 2.

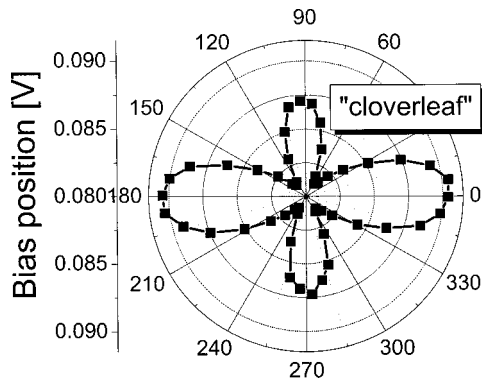


FIG. 3. Dependence of the peak bias position on the magnetic field direction in the plane of the quantum well for the  $X_{XY}(1) \rightarrow X_{XY}(1)$  resonance of a 60–40–60 sample at 12 kbar demonstrating clear “cloverleaf” symmetry. In this case the outside interface between the collector AlAs well and the GaAs contact layer was doped with  $\sim 0.9$  ml of InAs, but this does not appear to have a noticeable effect on the symmetry of the results. Note that the bias scale goes to roughly half the range of that for the inset of Fig. 2 (which plots the separation between peaks in both bias directions) and it is also expanded to enhance the appearance of the cloverleaf.

Figure 2 shows that the  $m=1$  resonance bias position depends on the field angle. The voltage separation of the resonance peaks in forward and reverse bias (=twice the average of the absolute bias values) is plotted as a function of field angle in the inset. It displays an elliptical polar dependence, with a ratio of major to minor axes of 1.23. Similar ratios of  $1.22 \pm 0.02$  were observed at 15 T in another 70–40–70 sample from the same wafer and a 60–40–60 sample.

Note that Fig. 2 exhibits twofold symmetry rather than the fourfold cloverleaf symmetry that would be expected due to contributions from both  $X_X$  and  $X_Y$  conduction band minima. It can be attributed to the existence of a small, uniaxial stress component in the pressure cell, estimated to be  $\leq 0.5$  kbar,<sup>16</sup> which splits the  $X_X$  and  $X_Y$  minima, causing only the lowest pair of minima in the emitter to be occupied.<sup>17</sup> This is confirmed by the successful observation of a cloverleaf for some samples when cooled very slowly in the same cell.<sup>18</sup> An example is shown in Fig. 3.

Only a single resonant peak is observed in Fig. 2 for the (100) direction. It corresponds to the dispersion of the camel-back minimum going away from the  $X$  point. The lower energy dispersion in the opposite direction is not observed. We believe this is because its bias is very small compared with the width of the resonance; the corresponding current will also be small. It can be seen from the estimated ambient pressure camel-back dispersion shown below in Fig. 4 (inset) that the dispersion energy relative to the camel-back minimum going  $0.02 \times 2\pi/a$  towards the  $X$  point is  $\sim 1$  meV and is about  $5 \times$  smaller than that going the same distance away from the  $X$  point. The camel back becomes even shallower at 10 kbar, making this ratio even larger and further reducing the dispersion energy in the direction of the  $X$  point. In addition, using the self-consistent Schrödinger-Poisson analysis described in Ref. 11, we estimate that about  $2 \times 10^{11} \text{ cm}^{-2}$  electrons are present in the camel-back minimum of the emitter AlAs well at 9 kbar, which gives the emitter Fermi

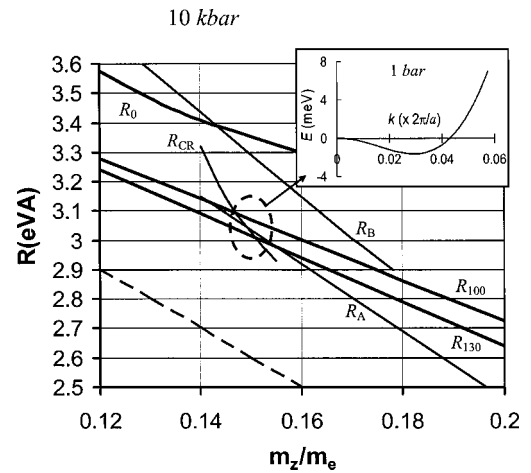


FIG. 4. Fits at 10 kbar of  $R(m'_z)$  to the data in Fig. 2 (inset) for offset voltages of  $V=0, 100,$  and  $130$  mV ( $R_V$ ), to measurements of Landau level splittings at 10 kbar ( $R_A$  and  $R_B$ ), and to 1 bar high field cyclotron resonance data ( $R_{CR}$ ). For  $R_{CR}$ , the pressure difference was taken into account by shifting  $m'_z$  as described in the text. The dashed line is a fit to the data in Fig. 2 (inset) under the assumption of no camel back. The dashed ellipse shows the unique intersection point for all three sets of data. **Inset:** The dispersion at ambient pressure, deduced from the values at the intersection point, which clearly exhibits a camel back.

surface a diameter of about  $0.02 \times 2\pi/a$  along the camel-back direction. This diameter is not much smaller than the position of the camel-back minimum at 10 kbar (it reduces by  $\sim 0.01 \times 2\pi/a$  at 10 kbar). Thus, the broadening of the lower energy resonance is comparable with its bias position, almost certainly rendering this resonance unobservable.

The camel-back dispersion in the  $z$  direction for the  $X_Z$  valleys is described by the eigenvalue,  $E(k_z)$ , of the Hamiltonian  $\underline{H}(k_z) = \underline{I}(\hbar^2 k_z^2 / 2m'_z) - \underline{\sigma}_z [\Delta / 2] - i \underline{\sigma}_y R k_z$ , where  $\underline{\sigma}_y, \underline{\sigma}_z$  are Pauli spin matrices,  $\Delta$  is the  $X_1$ - $X_3$  energy splitting, and  $R = -(\hbar^2 / m_0) \langle u_1 | d/dz | u_3 \rangle$  is the  $\mathbf{k} \cdot \mathbf{p}$  interaction in which  $u_1$  and  $u_3$  are the  $X_1$  and  $X_3$  crystal periodic functions. The dispersion of the same  $X_Z$  valleys in the  $x$ - and  $y$  directions is unaffected by any  $\mathbf{k} \cdot \mathbf{p}$  interaction and has a parabolic dependence on wave vector, with effective mass  $m_{X,Y}$ . This effective mass was recently measured as a function of pressure and reported to be  $m_{X,Y}/m_0 = 0.284 - 0.0039P$ , where  $P$  is the pressure in kbar and  $m_0$  is the free-electron mass.<sup>19</sup> Currently accepted values of the  $\mathbf{k} \cdot \mathbf{p}$  parameters  $R = 1 \text{ eV \AA}$  and  $m'_z = 1.56m_0$  thus yield a value of approximately 4.5 for the ratio of constant energy surface axes and a predicted mass ratio of 20.<sup>20,21</sup> This mass ratio is well outside that observed in Fig. 2 (inset), suggesting that  $R$  and  $m'_z$ , must be re-evaluated. Such a re-evaluation is also consistent with a recent observation of interface induced  $X_X$ - $X_Y$  band mixing by some of the authors.<sup>12</sup> In order to achieve acceptable values for the interface mixing potentials, it was required that  $R > 2.5 \text{ eV \AA}$ . This issue will be considered in more detail below.

It is in fact not possible to determine  $R$  and  $m'_z$  from the shape of the constant energy surface alone. Instead, we can find a function,  $R_0(m'_z)$  that gives a good fit to the observed angle dependence of bias shift in the inset of Fig. 2. The

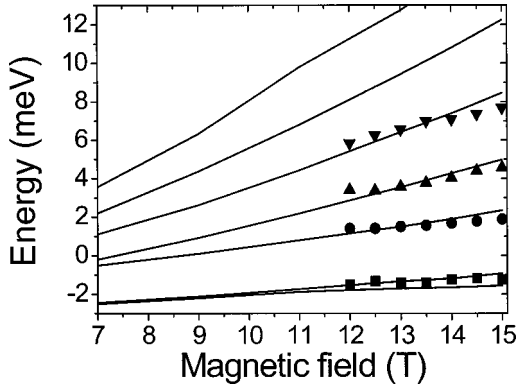


FIG. 5. Fan of  $X_{X,Y}$  Landau levels in a GaAs/AlAs double-barrier structure at a pressure of 10 kbar: experimental data from Ref. 22 (symbols) and best fit using method in Ref. 23 (solid lines).

resulting function  $R_0(m'_z)$  is plotted against  $m'_z$  in Fig. 4. However, we can also fit  $X_{X,Y}$  Landau levels measured by some of the authors at  $\sim 10$  kbar (Ref. 22) to a model that includes the  $\mathbf{k} \cdot \mathbf{p}$  interaction;<sup>23</sup> this yields two *different* functions,  $R_A(m'_z)$  and  $R_B(m'_z)$ , depending, respectively, on whether or not the splitting between the first two Landau levels is resolved in the measurements. An example of when the splitting is not resolved is shown in Fig. 5 for the point  $R=3.39$  eV  $\text{\AA}$  and  $m'_z=0.142m_0$ . This lack of resolution is only reasonable for  $R > 2.9$ , so  $R_B(m'_z)$  only exists for  $R > 2.9$ .<sup>18,24</sup> On the other hand, for  $R_A(m'_z)$  the quality of the fit is only good for  $R < 3.2$ , because when  $R=3.2$  the standard deviation is then about 30% of the typical Landau level separation, but decreases at smaller  $R$  values. Thus,  $R_A(m'_z)$  only exists for  $R < 3.2$ . As shown in Fig. 4,  $R_0(m'_z)$  intersects only with  $R_B(m'_z)$ , and this gives a unique pair of values for  $R$  and  $m'_z$  at  $\sim 10$  kbar of  $3.4$  eV  $\text{\AA}$  and  $0.142m_0$ , respectively. If we further assume that  $R$  is essentially independent of pressure (since different III-V materials have similar  $\mathbf{k} \cdot \mathbf{p}$  interaction parameters<sup>25</sup> and hydrostatic pressure does not affect the symmetry), and that  $m'_z$  exhibits a similar relative pressure dependence to that quoted above for  $m_{X,Y}$ ,<sup>19</sup> we can estimate the values of  $R$  and  $m'_z$  at ambient pressure. We find  $R=3.4$  eV  $\text{\AA}$  and  $m'_z=0.16m_0$ .

Based on these new  $\mathbf{k} \cdot \mathbf{p}$  parameters, we have calculated the shape of the camel back from the above Hamiltonian and found that the largest dispersion energy at the experimental wave vector  $k \sim (0.022 \times 2\pi/a_0)$  is  $\sim 10$  meV, in fact perpendicular to the axis of the camel back. If all the applied bias were dropped between the two AlAs wells then twice this value, or 20 meV, should equal the maximum peak separation in Fig. 2 (inset), which clearly is not the case. Even if we assume that the collector AlAs well is fully depleted, an estimate of the associated depletion in the GaAs contact layer adjacent to the collector (as in Ref. 11) shows that this would only increase the resonance bias at 15 T by a factor of  $\sim 2.5$ , and the peak separation in Fig. 2 (inset) would then be  $\sim 50$  mV. Instead, the maximum separation is  $\sim 150$  mV. This suggests that an offset,  $100 < V < 130$  mV, must first be subtracted from the data in Fig. 2 (inset). A consequence is that the mass anisotropy increases to  $3.0 \pm 0.6$ , and the constant energy surface anisotropy lies in the range  $1.7 \pm 0.2$ .

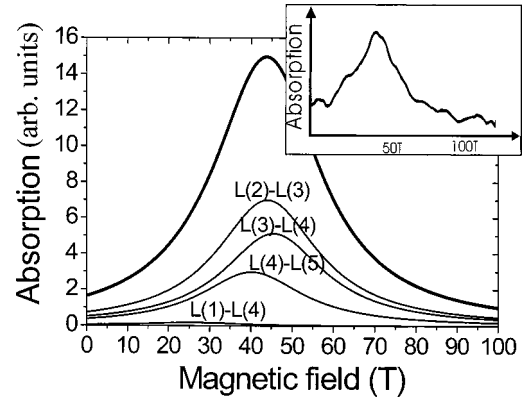


FIG. 6. Cyclotron resonance measurement at ambient pressure on AlAs at 145 K from Ref. 26 (inset) and best fit for  $m'_z=0.16m_0$  which occurs at  $R=3.4$  eV  $\text{\AA}$ . All transitions between different Landau levels,  $L(i)$ , with  $i=1,2,3,\dots$ , are shown that contribute to the final peak. An empirical broadening parameter has been used.

Although the origin of the offset is not clear, it could be due, for example, to the formation of Landau levels in the bulk GaAs contacts that will increase the barrier,  $\delta$ , in Fig. 1 by half the GaAs cyclotron energy, or 13 meV. An offset that is independent of field angle would then arise because of the extra bias required for injection of carriers into the emitter AlAs well and for their removal, by tunneling, from the collector AlAs well. This explanation is also consistent with the absence of any offset for the  $m=3$  resonance discussed below, which occurs at a much larger perpendicular electric field and which shows only small magnetic field induced shifts which do not depend on pressure.

If we subtract the offset before fitting the  $\mathbf{k} \cdot \mathbf{p}$  parameters in Fig. 2 (inset), we obtain a function  $R_V(m'_z)$  that intersects now only with  $R_A(m'_z)$ . The extreme cases,  $R_{100}(m'_z)$  and  $R_{130}(m'_z)$ , are plotted in Fig. 4 for offsets of  $V=100$  and  $130$  mV, respectively. The point of intersection, shown by the dashed ellipse in Fig. 4, yields slightly different *ambient pressure*  $\mathbf{k} \cdot \mathbf{p}$  parameters,  $R=3.1 \pm 0.1$  eV  $\text{\AA}$  and  $m'_z=0.17 \pm 0.01 m_0$ . Allowing for the offset, we now have a self-consistent analysis in which the potential drop in the active region of the device agrees with the dispersion energy calculated from the deduced  $\mathbf{k} \cdot \mathbf{p}$  parameters.

The new values  $R=3.1 \pm 0.1$  eV  $\text{\AA}$  and  $m'_z=0.17 \pm 0.01 m_0$  also agree very well with the intersection of a third function,  $R_{CR}(m'_z)$ , deduced by fitting the ambient pressure cyclotron resonance data of Miura *et al.*<sup>26,27</sup> and then shifting  $m'_z$  by  $\sim -0.02 m_0$  as described above to account for the change between ambient pressure and 10 kbar. An example of the relative contribution from different transitions between Landau levels,  $L(i) \rightarrow L(j)$ , is shown in Fig. 6 for one set of  $R$  and  $m'_z$  that contributes to the curve  $R_{CR}(m'_z)$ . This calculation was carried out using the method described in Ref. 23. Each transition strength is weighted by the thermal occupation of the initial level and the oscillator strength for the transition which includes both X1 and X3 contributions. In Fig. 4 it can be seen that  $R_{CR}(m'_z)$  intersects with the two curves from parallel and perpendicular magneto-tunneling experiments at 10 kbar at the same point as they

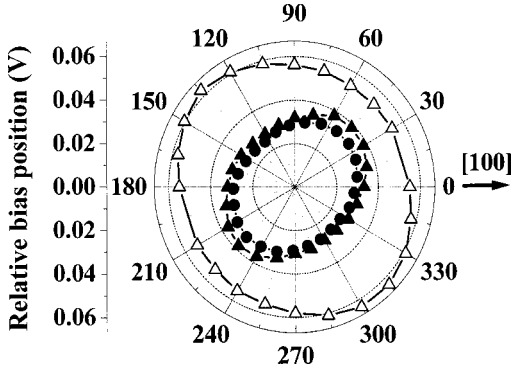


FIG. 7. Angle dependence of the field induced shift in a 60–40–60 sample at 4.2 K and 15 T for the  $X_{XY}(1) \rightarrow X_{XY}(3)$  resonance peak in forward bias at 1 bar (solid triangle), in reverse bias at 1 bar (open triangle), and in forward bias at 10 kbar (solid circle).

intersect with each other. This therefore also provides some additional support for the shift of  $m'_z$  by  $\sim -0.02 m_0$  to account for the effect of applying a pressure of 10 kbar. We conclude that the intersection of the  $R$  vs  $m'_z$  curves from three independent sets of data provides very strong evidence for our new values. They correspond to a camel back at ambient pressure with position,  $k_0 \sim 0.03 \times 2\pi/a_0$ , and depth,  $\delta_0 \sim 1.6$  meV (see the inset to Fig. 4).

It is also possible to derive  $R(m'_z)$  by assuming no camel back (dashed line in Fig. 4). However, in this case  $R(m'_z)$  has no intersection in the range of interest with any of  $R_A(m'_z)$ ,  $R_B(m'_z)$ , or  $R_{CR}(m'_z)$ , so the assumption must be incorrect. Our results therefore prove fairly conclusively that a camel back must exist in AIs. The shallow depth of the camel back deduced above,  $\delta_0 \sim 1.6$  meV, may perhaps account for the severe difficulty that this region of the AIs band structure has presented in the past to both theoretical and experimental physicists wishing to make a clear identification of its camel-back character.

### B. Interface induced $X_X$ - $X_Y$ band mixing

Figure 7 shows the angle dependence of the  $m=3$  resonance for the 60–40–60 sample at 4.2 K in both bias directions at ambient pressure and in forward bias at 10 kbar. In contrast to the  $m=1$  resonance, the field induced shift is now much smaller than the zero field peak position, and there does not appear to be the same field induced offset that was observed for  $m=1$ . The angle dependence is elliptical, with its major axis now clearly oriented now along a  $[110]$  direction. At 10 kbar, the ratio of major to minor axes is now  $\sim 1.4$  and  $\sim 1.2$ , respectively, in forward and reverse bias, increasing very slightly at 1 bar. It can also be seen that the orientation of the major axis rotates by  $90^\circ$  when the bias is reversed.

The change of the constant energy surface from elongation along the  $\langle 100 \rangle$  directions for  $m=1$  to an elliptical surface oriented along a single  $\langle 100 \rangle$  direction for  $m=3$  is due to  $X_X$ - $X_Y$  interface band mixing, as recently described in Ref. 12. In an ideal sample, the Ga–As bonds at adjacent interfaces of an AIs quantum well lie in the  $[110]$  and  $[\bar{1}10]$

planes, respectively. When an electric field is applied in the  $z$  direction, it breaks the symmetry and the effective masses in the  $[110]$  and  $[\bar{1}10]$  directions can then be different. Moreover, on reversing the electric field in an ideal sample, the effective masses in the two  $\langle 110 \rangle$  directions will be interchanged, resulting in a  $90^\circ$  rotation of the mass ellipse. This is indeed the behavior observed in Fig. 7 for the  $m=3$  resonance. Analogous but weaker mass anisotropy has been observed recently for  $\Gamma$  electrons in GaAs/AlAs quantum wells.<sup>28</sup>

As described in detail in Ref. 29, it is possible to use the shape of the angle dependence of the  $X_{X,Y}(3)$  resonance in Fig. 7 to estimate values for the interface band mixing potentials in the collector well corresponding to states of  $X_1$  and  $X_3$  symmetry, respectively. These are found to be  $\bar{V}_1^{X-Y} \sim 45$  meV and  $\bar{V}_3^{X-Y} \sim 15$  meV. Because these potentials depend on the electric field in the collector well, we must rescale their values using the appropriate  $X_{X,Y}$  envelope functions, as described after Eq. (2) in Ref. 12, to obtain  $\bar{V}_1^{X-Y} \sim 5$  meV and  $\bar{V}_3^{X-Y} \sim 3$  meV for the  $X_{X,Y}(1)$  resonance.<sup>30</sup> The effect of the interface band mixing is to change the dispersion at the  $X$  point according to the following perturbing Hamiltonian presented in Ref. 12:  $\underline{H}_{IF}(k_x, k_y) = \underline{I}E_+ + \underline{\sigma}_z \times (E_- - \varepsilon/2) + \underline{\sigma}_x V(k_x, k_y)$ , in which  $E_\pm = [E(k_x) \pm E(k_y)]/\sqrt{2}$ ,  $\varepsilon$  is the uniaxial stress splitting of the  $X_X$  and  $X_Y$  states, and  $V(k_x, k_y) = b^*(k_x)b(k_y)\bar{V}_1^{X-Y} + a^*(k_x)a(k_y)\bar{V}_3^{X-Y}$ , where  $[b(k_z), a(k_z)]$  is the eigenvector of the Hamiltonian,  $\underline{H}(k_z)$ , defined above. We have verified that for  $0 < \varepsilon \leq 5$  meV,  $\underline{H}_{IF}$  has little effect on the dispersion of the  $X_X(1)$  sub-band within the experimental wave-vector range of 0.02 from the camel-back minimum. To ignore it would cause changes in the fitted values of both  $R$  and  $m'_z$  of less than 3%. Thus, the earlier analysis of the angle dependence of the resonant tunneling peak separation for the first resonance, based on the data in the inset of Fig. 2, which confirmed the existence of the camel back and yielded new values for the  $\mathbf{k} \cdot \mathbf{p}$  parameters, remains valid even though it was based only on  $\underline{H}(k_z)$ , which ignores interface band mixing.

### III. CONCLUSION

In conclusion, we have measured directly the dimensions of the constant energy surface at the conduction band minimum in AIs. Our measurements provide direct evidence for the existence of a camel back. The constant energy surface is much more spherical than expected, with its axis ratio in the range  $1.7 \pm 0.2$ , leading to a major re-evaluation of the  $\mathbf{k} \cdot \mathbf{p}$  parameters at the  $X$  point. In particular, the energy parameter  $R = 3.0 \pm 0.1$  eV Å is increased by a factor of 3. Without this increase, it would not be possible to explain the rotation we have observed in a perpendicular electric field of the principal dispersion axes in an AIs quantum well. At low fields the camel back dominates, but in high fields the effect of  $X_X$ - $X_Y$  mixing becomes significant, creating a new conduction band minimum at the  $X$  point whose principal axes are

rotated by  $\pi/4$ . We have shown that the sign of the rotation depends on the sign of the electric field. This behavior is a direct consequence of the large  $X_3$  contribution to the ground-state wave function, produced by the strong  $\mathbf{k}\cdot\mathbf{p}$  interaction.

## ACKNOWLEDGMENTS

This work was funded by E.P.S.R.C. of the U.K. H. Im and L.E.B. acknowledge support from the QSRC at Dongguk University and the Rhodes Trust, respectively.

- 
- \*Presently at the Department of Semiconductor Science, Dongguk University, Seoul, Korea.
- †Presently at SCD, Haifa 31021, Israel.
- <sup>1</sup>P. Lawaetz, *Solid State Commun.* **16**, 65 (1975).
- <sup>2</sup>D. Bimberg, W. Bludau, R. Linnebach, and E. Bauser, *Solid State Commun.* **37**, 987 (1981).
- <sup>3</sup>M.J. Steer, D.A. Carder, L.R. Wilson, J.W. Cockburn, M. Hopkinson, C.K. Chia, R. Airey, and G. Hill, *Electron. Lett.* **37**, 1292 (2001).
- <sup>4</sup>G. Grosso and C. Piermarocchi, *Phys. Rev. B* **51**, 16 772 (1995).
- <sup>5</sup>K. Rim *et al.* and L.J. Huang *et al.*, Proceedings 2001 IEEE VLSI Symposium, Kyoto, Japan (unpublished).
- <sup>6</sup>M.Z. Huang and W.Y. Ching, *J. Phys. Chem. Solids* **46**, 977 (1985).
- <sup>7</sup>E. Hess, I. Topol, K.-R. Schultze, H. Neumann, and K. Unger, *Phys. Status Solidi B* **55**, 187 (1973).
- <sup>8</sup>A.A. Kopylov, *Solid State Commun.* **56**, 1 (1985).
- <sup>9</sup>Y.-T. Lu and L.J. Sham, *Phys. Rev. B* **40**, 5567 (1989).
- <sup>10</sup>B.A. Foreman, *Phys. Rev. Lett.* **81**, 425 (1998).
- <sup>11</sup>J.M. Smith, P.C. Klipstein, R. Grey, and G. Hill, *Phys. Rev. B* **57**, 1740 (1998).
- <sup>12</sup>H. Im, P.C. Klipstein, R. Grey, and G. Hill, *Phys. Rev. Lett.* **83**, 3693 (1999).
- <sup>13</sup>J. Smoliner, W. Demmerle, G. Berthold, E. Gornik, G. Weimann, and W. Schlapp, *Phys. Rev. Lett.* **63**, 2116 (1989).
- <sup>14</sup>R.K. Hayden, D.K. Maude, L. Eaves, E.C. Valadares, M. Henini, F.W. Sheard, O.H. Hughes, J.C. Portal, and L. Cury, *Phys. Rev. Lett.* **66**, 1749 (1991).
- <sup>15</sup>P.C. Klipstein, *High Pressure Semiconductor Physics II*, Semiconductors and Semimetals, edited by T. Suski and W. Paul (Academic, New York, 1998), Vol. 55, p. 45.
- <sup>16</sup>A. Kornilov (unpublished).
- <sup>17</sup>W.R. Tribe, P.C. Klipstein, G.W. Smith, R. Grey, and J.S. Roberts, *J. Phys. Chem. Solids* **56**, 429 (1995).
- <sup>18</sup>L. Bremme, D.Phil. thesis, Oxford University (2001); L. Bremme (to be published).
- <sup>19</sup>H. Im, P.C. Klipstein, R. Grey, and G. Hill, *Phys. Rev. B* **62**, 11 076 (2000).
- <sup>20</sup>O. Madelung, *Semiconductors—Basic Data*, 2nd revised ed. (Springer, Berlin, Heidelberg, New York, 1996), p. 76.
- <sup>21</sup>Y. Fu, M. Willander, E.L. Ivchenko, and A.A. Kiselev, *Phys. Rev. B* **47**, 13 498 (1993).
- <sup>22</sup>J.M. Smith, P.C. Klipstein, R. Grey, and G. Hill, *Phys. Rev. B* **57**, 1746 (1998).
- <sup>23</sup>L.E. Bremme and P.C. Klipstein, Proceedings 25th Int. Conf. Phys. Semicond., Osaka, September 2000 (unpublished); *Phys. Rev. B* **66**, 235316 (2002).
- <sup>24</sup>L.E. Bremme, H. Im, H. Choi, G.W. Smith, R. Grey, and P.C. Klipstein, Proceedings 25th Int. Conf. Phys. Semicond., Osaka, September 2000 (unpublished).
- <sup>25</sup>G. Bastard, *Wave Mechanics Applied to Semiconductor Heterostructures* (Halstead, New York, 1988).
- <sup>26</sup>N. Miura, G. Kido, M. Suekane, and S. Chikazume, *J. Phys. Soc. Jpn.* **52**, 2838 (1983).
- <sup>27</sup>The fit could only be made by assuming the main CR line at  $\sim 40$  T does not include the transition between the lowest two Landau levels. This transition is predicted at  $\sim 80$  T and was not observed. The reason could be field induced carrier freeze out, which is consistent with the absence of any signal below 120 K, even at 40 T.
- <sup>28</sup>T. Reker, H. Im, L.E. Bremme, H. Choi, Y. Chung, P.C. Klipstein, and H. Shtrikman, *Phys. Rev. Lett.* **88**, 056403 (2002).
- <sup>29</sup>H. Im, L.E. Bremme, Y.C. Chung, P.C. Klipstein, R. Grey, and G. Hill, *Physica E (Amsterdam)* **6**, 214 (2000).
- <sup>30</sup>Rescaling is possible because  $X_{XY}(1)$  and  $X_{XY}(3)$  have the same parity in zero electric field, and because, at their respective resonances, the amplitudes of the  $X_{XY}(1)$  and  $X_{XY}(3)$  wave functions are nearly equal at each interface of the collector well.